FBMC-OQAM in Doubly-Selective Channels: A New Perspective on MMSE Equalization

Ronald Nissel†, Markus Rupp†, and Roman Marsalek‡
†Christian Doppler Laboratory for Dependable Wireless Connectivity for the Society in Motion, TU Wien, Vienna, Austria
‡The Faculty of Electrical Engineering and Communication, Brno University of Technology, Brno, Czech Republic
Email: rnissel@nt.tuwien.ac.at, mrupp@nt.tuwien.ac.at, marsaler@feec.vutbr.cz

***Abstract*—In many practical cases, one-tap equalizers achieve a close to optimum performance in filter bank multi-carrier modulation systems. However, if the channel is highly doubly-selective, that is, time-selective and frequency-selective, enhanced equalization methods might be necessary. In this paper, we generalize the n-tap Minimum Mean Squared Error (MMSE) equalization, proposed in literature, by also including neighboring subcarriers into the equalization process. As a reference, we also derive a full block MMSE equalizer and compare to a low-complexity interference cancellation scheme. Our investigation starts with a single-antenna system and is later extended to multiple antennas.**

***Index Terms*—FBMC-OQAM, Equalizer, MMSE, Interference Cancellation, MIMO**

I. Introduction

The poor spectral properties of Orthogonal Frequency Division Multiplexing (OFDM) are one of its biggest disadvantages. Filter Bank Multi-Carrier (FBMC) with Offset Quadrature Amplitude Modulation (OQAM), in short just FBMC, has lower out-of-band emissions than OFDM [1]. This, however, comes at the expense of sacrificing the complex orthogonality condition and replacing it by the less strict real orthogonality condition, requiring special treatment, especially for channel estimation [2] and some Multiple-Input and Multiple-Output (MIMO) techniques [3]–[5].

In most practical cases, the channel induced interference can be neglected compared to the noise, so that both, OFDM and FBMC, show the same performance in terms of Bit Error Ratio (BER) for a one-tap equalizer [6]. However, in some scenarios, especially in a high Signal-to-Noise Ratio (SNR) regime, interference may be dominant, so that sophisticated equalization methods become necessary.

Most papers dealing with equalization in FBMC assume a time-invariant channel [7]–[11]. Authors in [7] propose a parallel equalization scheme, requiring multiple parallel Fast Fourier Transform (FFT) blocks, while the equalization method in [9] requires a larger FFT. In our paper, we consider an equalization method that operates after a conventional FFT.

A Minimum Mean Squared Error (MMSE) equalization method was proposed in [10] for a time-invariant channel and later extended in [11] to MIMO. Authors in [12] considered the same method as in [10] but applied it in a doubly-selective channel. All those papers [10]–[12] consider the interference contribution of neighboring subcarriers only in a statistical sense. However, from a conceptional point of view, there is no difference between interference coming from neighboring time-symbols and interference coming from neighboring subcarriers. Thus, an equalizer which utilizes only neighboring time-symbols, but ignores neighboring subcarriers, is in many cases not optimal.

The novel contribution of our paper can be summarized as follows:

- In contrast to [10]–[12], our n-tap MMSE equalizer not only considers neighboring time-symbols, but also includes neighboring subcarriers.
- As a reference, we also consider a full block MMSE equalizer (high computational complexity) in addition to the n-tap MMSE equalizer.
- Finally, we propose a low-complexity interference cancellation scheme for FBMC and compare it to the n-tap MMSE equalization.

II. FBMC-OQAM

In FBMC, real-valued data symbols are transmitted over a rectangular time-frequency grid. Let us denote the transmitted data symbol at subcarrier position l and time-position k by $x_{l,k} \in \mathbb{R}$. The transmitted signal in the time domain, consisting of L subcarriers and K time-symols, can then be expressed by [1]:

$$s(t) = \sum_{k=1}^{K} \sum_{l=1}^{L} g_{l,k}(t)\, x_{l,k}. \tag{1}$$

The basis pulse $g_{l,k}(t)$ is, essentially, a time and frequency shifted versions of the prototype filter $p(t)$, that is,

$$g_{l,k}(t) = p(t - kT)\, \mathrm{e}^{\mathrm{j}2\pi\, lF\,(t-kT)}\, \mathrm{e}^{\mathrm{j}\frac{\pi}{2}(l+k)}. \tag{2}$$

Such multicarrier system is mainly characterized by the prototype filter as well as time spacing T and frequency spacing F. In FBMC, the prototype filter is designed to be complex orthogonal for a time-frequency spacing of $TF = 2$. To achieve maximum data rate, however, we reduced the time spacing and the frequency spacing by a factor of two each, leading to $TF = 0.5$. This causes interference which is shifted to the purely imaginary domain by the phase shift $\mathrm{e}^{\mathrm{j}\frac{\pi}{2}(l+k)}$. Due to this imaginary interference, only real-valued symbols can be transmitted.

The continuous-time representation in (1) helps us to understand the basic concept of FBMC. However, an efficient generation of such signal is only possible in the discrete-time domain. Furthermore, a discrete-time representation simplifies

978-1-5090-3009-5/17/$31.00

analytical investigations. We thus consider the sampled signal $\mathbf{s} \in \mathbb{C}^{N\times 1}$ of (1), which can be expressed by:

$$\mathbf{s} = \mathbf{G}\,\mathbf{x}, \tag{3}$$

with

$$\mathbf{G} = \begin{bmatrix} \mathbf{g}_{1,1} & \mathbf{g}_{2,1} & \cdots & \mathbf{g}_{L,1} & \mathbf{g}_{1,2} & \cdots & \mathbf{g}_{L,K} \end{bmatrix}, \tag{4}$$

$$\mathbf{x} = \begin{bmatrix} x_{1,1} & x_{2,1} & \cdots & x_{L,1} & x_{1,2} & \cdots & x_{L,K} \end{bmatrix}^{\mathsf{T}}. \tag{5}$$

Transmit matrix $\mathbf{G} \in \mathbb{C}^{N\times LK}$ is build-up by vector $\mathbf{g}_{l,k} \in \mathbb{C}^{N\times 1}$, representing the sampled basis pulses in (2), with N denoting the total number of samples in time. Data symbol vector $\mathbf{x} \in \mathbb{R}^{LK\times 1}$, on the other hand, stacks all the transmitted data symbols in a large vector. Note that in practice, (3) is generated by an IFFT and not by a matrix multiplication [1].

We model time-variant multipath propagation by a time-variant convolution matrix $\mathbf{H} \in \mathbb{C}^{N\times N}$. The received symbols $\mathbf{y} \in \mathbb{C}^{LK\times 1}$ are obtained by matched filtering (for AWGN), that is, multiplying the received samples by $\mathbf{G}^{\mathsf{H}}$. Thus, the overall transmission system can be expressed by:

$$\mathbf{y} = \mathbf{D}\,\mathbf{x} + \mathbf{G}^{\mathsf{H}}\mathbf{n}, \tag{6}$$

with transmission matrix $\mathbf{D} \in \mathbb{C}^{LK\times LK}$ defined as

$$\mathbf{D} = \mathbf{G}^{\mathsf{H}}\,\mathbf{H}\,\mathbf{G}, \tag{7}$$

and $\mathbf{n} \sim \mathcal{CN}(\mathbf{0}, P_{\mathrm{n}}\,\mathbf{I}_N)$ representing the white Gaussian noise with P_{n} denoting the noise power in the time domain. Note that real orthogonality in FBMC implies that $\Re\{\mathbf{G}^{\mathsf{H}}\mathbf{G}\} = \mathbf{I}_{LK}$. In practice, (7) has to be estimated by pilots, similar as in [13]. Although we consider a block transmission of L subcarriers and K time-symbols, our matrix based system model can easily be extended to describe infinitely many transmission blocks, see for example [3].

III. Equalization

In many practical scenarios, the off-diagonal elements of $\mathbf{D}$, see (6) and (7), are so small, that they are dominated by the noise. A simple one-tap Zero Forcing (ZF) equalizer, $\frac{y_{l,k}}{h_{l,k}}$, with $h_{l,k}$ representing the appropriate diagonal element of $\mathbf{D}$, is then sufficient to achieve a close to optimal symbol detection probability. For white Gaussian noise, a one-tap ZF equalizer even corresponds to the maximum likelihood symbol detection. This explains why one-tap equalizers are so useful in practice. However, in highly doubly-selective channels and if we operate in a high SNR regime, one-tap equalizers might not be sufficient anymore. To better illustrate this fact, let us consider a one-tap equalizer in case of a Vehicular A channel model and a Jakes-Doppler spectrum with a maximum Doppler shift of 1.16 kHz (500 km/h for a carrier frequency of 2.5 GHz). Furthermore, we assume a subcarrier spacing of $F = 15$ kHz. This parameters lead to a channel induced Signal-to-Interference Ratio (SIR) of 20 dB for the PHYDYAS prototype filter [14]. As illustrated in Fig. 1, only a few close symbols in time and frequency contribute significantly to the SIR. Similar, Fig. 2 shows the interference distribution for the Hermite prototype filter [15], [16]. The total SIR is 23 dB and thus better than for the PHYDYAS filter. From both figures, we conclude that the underlying prototype filter has a huge impact on which neighboring symbols cause interference.

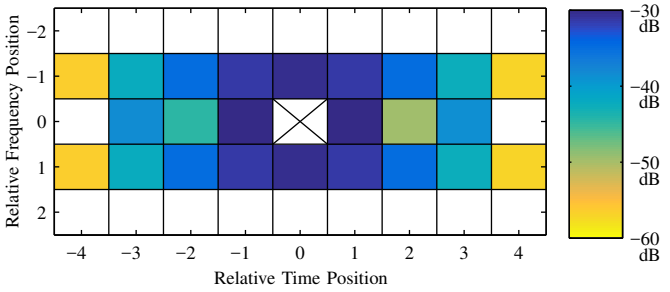

Fig. 1. The interference contribution of neighboring symbols for the **PHYDYAS** prototype filter. Only a few symbols have a significant contribution to the total interference (SIR=20 dB).

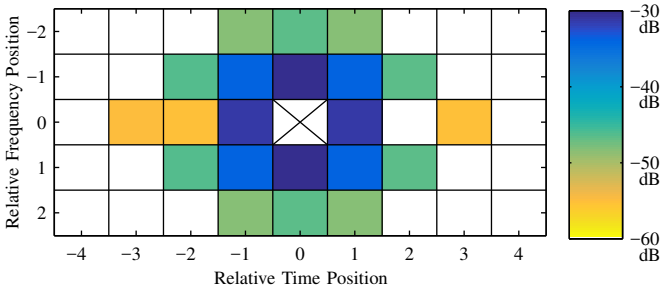

Fig. 2. Same as in Fig. 1 but for a **Hermite** prototype filter. The total SIR is 23 dB and thus better than for the PHYDYAS prototype filter. Furthermore, we see a rather symmetric interference contribution because the Hermite prototype filter is symmetric in time and frequency.

Throughout the paper, we will consider the same channel model (Vehicular A, Jakes Doppler spectrum with a maximum Doppler shift of 1.16 kHz). The subcarrier spacing is set to $F = 15$ kHz and the number of subcarriers to $L = 24$. For FBMC, we consider $K = 30$ time-symbols and for OFDM $K = 14$ symbols (Cyclic Prefix (CP) length of 4.7 μs), leading to the same transmission time for both schemes ($KT = 1$ ms). The Pulse-Amplitude Modulation (PAM) modulation order is set to 16, equivalent to a 256-Quadrature Amplitude Modulation (QAM) signal constellation. For such channel parameters, one-tap equalizers might not be sufficient anymore if the SNR is higher than approximately 10 dB. We thus require more sophisticated equalization methods.

A. MMSE

A simple way to estimate the transmitted data symbol vector $\mathbf{x}$ would be the employment of a conventional (complex-valued) MMSE equalizer. Unfortunately, this does not work because such equalizer would also include the imaginary interference into the minimization problem, leading to large detection errors. To avoid this problem, we stack real and imaginary part in a large vector, as suggested in [10]. The full block MMSE equalization of $\mathbf{y}$, see (6), can then be calculated by:

$$\hat{\mathbf{x}} = \begin{bmatrix} \Re\{\mathbf{D}\} \\ \Im\{\mathbf{D}\} \end{bmatrix}^{\mathsf{T}} \left(\begin{bmatrix} \Re\{\mathbf{D}\} \\ \Im\{\mathbf{D}\} \end{bmatrix} \begin{bmatrix} \Re\{\mathbf{D}\} \\ \Im\{\mathbf{D}\} \end{bmatrix}^{\mathsf{T}} + \mathbf{\Gamma} \right)^{-1} \begin{bmatrix} \Re\{\mathbf{y}\} \\ \Im\{\mathbf{y}\} \end{bmatrix}, \tag{8}$$

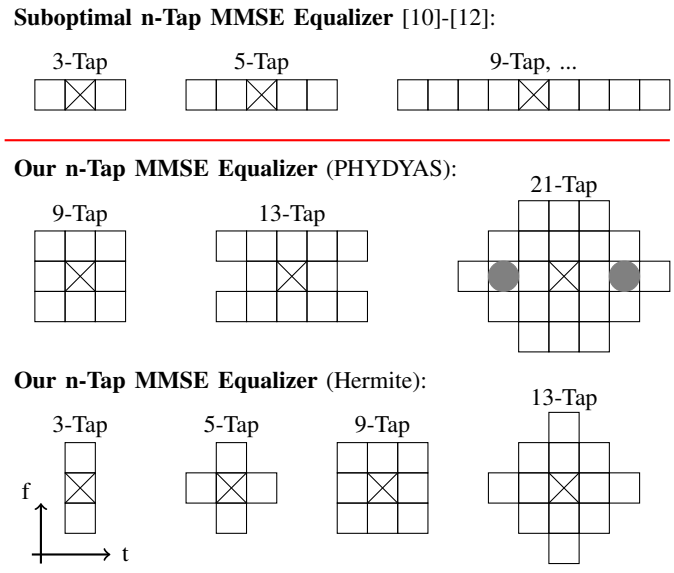

Fig. 3. The n-tap equalizer utilizes n received symbols to estimate the transmitted data symbol at one time-frequency position (indicated by the crosses in the center). Authors in [10]–[12] only employ neighboring time-symbols for the equalization process. This is, in many cases, not optimal.

with

$$\mathbf{\Gamma} = \frac{P_n}{2}\begin{bmatrix} \Re\{\mathbf{G}^{\mathsf{H}}\mathbf{G}\} & -\Im\{\mathbf{G}^{\mathsf{H}}\mathbf{G}\} \\ \Im\{\mathbf{G}^{\mathsf{H}}\mathbf{G}\} & \Re\{\mathbf{G}^{\mathsf{H}}\mathbf{G}\} \end{bmatrix}. \tag{9}$$

We might need the pseudo inverse in (8) because the matrix inversion is not always possible due to the time-frequency squeezing. However, there are two other main problems with the full block MMSE equalizer: Firstly, it has a high computational complexity. We have to invert a matrix of size $2LK \times 2LK$, too large for most practical applications. Secondly, a large delay is introduced because all symbols need to be received before performing the equalization. We therefore investigate an n-tap MMSE equalizer which includes only a few neighboring symbols. Let us split the transmission model of (6) according to:

$$\mathbf{y}_{\mathcal{S}} = \mathbf{D}_{\mathcal{S}}\mathbf{x}_{\mathcal{S}} + \mathbf{D}_{\mathcal{S},\mathcal{R}}\mathbf{x}_{\mathcal{R}} + \mathbf{n}_{\mathcal{S}}. \tag{10}$$

Here, $\mathbf{y}_{\mathcal{S}} \in \mathbb{C}^{|\mathcal{S}|\times 1}$ is a subvector of $\mathbf{y}$ with $\mathcal{S}$ representing the considered subblock, that is, certain time-frequency positions, see Fig. 3. For example, a subblock vector of size $|\mathcal{S}| = 5$ (5-tap) can be written as: $\mathbf{y}_{\mathcal{S}} = \begin{bmatrix} y_{l,k-2} & y_{l,k-1} & y_{l,k} & y_{l,k+1} & y_{l,k+2} \end{bmatrix}^{\mathsf{T}}$. Such subblock was used in [10] and only includes neighboring symbols in time but ignores neighboring subcarriers. In many cases, this is not optimal, especially in high velocity scenarios and for some specific prototype filters. Our considered subblock vector, on the other hand, can be expressed by $\mathbf{y}_{\mathcal{S}} = \begin{bmatrix} y_{l,k-1} & y_{l-1,k} & y_{l,k} & y_{l+1,k} & y_{l,k+1} \end{bmatrix}^{\mathsf{T}}$, see Fig. 3. Vector $\mathbf{x}_{\mathcal{S}} \in \mathbb{R}^{|\mathcal{S}|\times 1}$ in (10) represents the transmitted data symbols of the considered subblock, while $\mathbf{x}_{\mathcal{R}} \in \mathbb{R}^{|\mathcal{R}|\times 1}$ represents all other transmitted data symbols, relevant for $\mathbf{y}_{\mathcal{S}}$. Only a few symbols outside the subblock have a significant contribution on $\mathbf{y}_{\mathcal{S}}$, so that usually $|\mathcal{R}| << LK - |\mathcal{S}|$. The matrices $\mathbf{D}_{\mathcal{S}} \in \mathbb{C}^{|\mathcal{S}|\times|\mathcal{S}|}$ and $\mathbf{D}_{\mathcal{S},\mathcal{R}} \in \mathbb{C}^{|\mathcal{S}|\times|\mathcal{R}|}$ correspond to the correct elements of $\mathbf{D}$, so that (10) satisfies (6). Similar to (8), the $|\mathcal{S}|$-tap MMSE equalization of (10) becomes

$$\hat{\mathbf{x}}_{\mathcal{S}} = \begin{bmatrix} \Re\{\mathbf{D}_{\mathcal{S}}\} \\ \Im\{\mathbf{D}_{\mathcal{S}}\} \end{bmatrix}^{\mathsf{T}} \left(\mathbf{\Delta}_{\mathcal{S}} + \mathbf{\Delta}_{\mathcal{S},\mathcal{R}} + \mathbf{\Gamma}_{\mathcal{S}} \right)^{-1} \begin{bmatrix} \Re\{\mathbf{y}_{\mathcal{S}}\} \\ \Im\{\mathbf{y}_{\mathcal{S}}\} \end{bmatrix} \tag{11}$$

with

$$\mathbf{\Delta}_{\mathcal{S}} = \begin{bmatrix} \Re\{\mathbf{D}_{\mathcal{S}}\} \\ \Im\{\mathbf{D}_{\mathcal{S}}\} \end{bmatrix} \begin{bmatrix} \Re\{\mathbf{D}_{\mathcal{S}}\} \\ \Im\{\mathbf{D}_{\mathcal{S}}\} \end{bmatrix}^{\mathsf{T}} \tag{12}$$

$$\mathbf{\Delta}_{\mathcal{S},\mathcal{R}} = \begin{bmatrix} \Re\{\mathbf{D}_{\mathcal{S},\mathcal{R}}\} \\ \Im\{\mathbf{D}_{\mathcal{S},\mathcal{R}}\} \end{bmatrix} \begin{bmatrix} \Re\{\mathbf{D}_{\mathcal{S},\mathcal{R}}\} \\ \Im\{\mathbf{D}_{\mathcal{S},\mathcal{R}}\} \end{bmatrix}^{\mathsf{T}}. \tag{13}$$

Noise matrix $\mathbf{\Gamma}_{\mathcal{S}} \in \mathbb{C}^{2|\mathcal{S}|\times 2|\mathcal{S}|}$ in (11) is given by the submatrix of $\mathbf{\Gamma} \in \mathbb{C}^{2LK\times 2LK}$, see (9), corresponding to the correct elements. Note that $\hat{\mathbf{x}}_{\mathcal{S}}$ in (11) delivers in total $|\mathcal{S}|$ estimates. However, we are only interested in the center position, as illustrated in Fig. 3. The remaining elements are discarded. Thus, we require in total LK matrix inversions of size $2|\mathcal{S}| \times 2|\mathcal{S}|$. The computational complexity is usually lower then for the full block MMSE equalizer but still relatively high. In the next subsection, we propose a low-complexity interference cancellation scheme. But first, let us investigate the performance of the MMSE equalizers.

Fig. 4 shows how the BER depends on the SNR for the

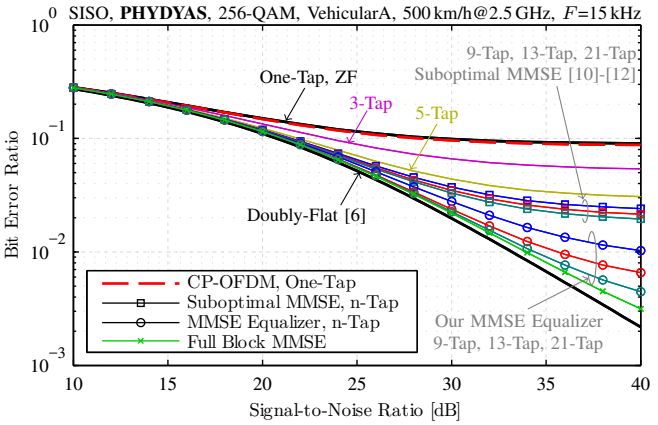

Fig. 4. Considering only neighboring time-symbols [10]–[12] is very inefficient. Instead, we utilize neighboring subcarriers as well, see Fig. 3. This greatly improves the performance of an n-tap equalizer.

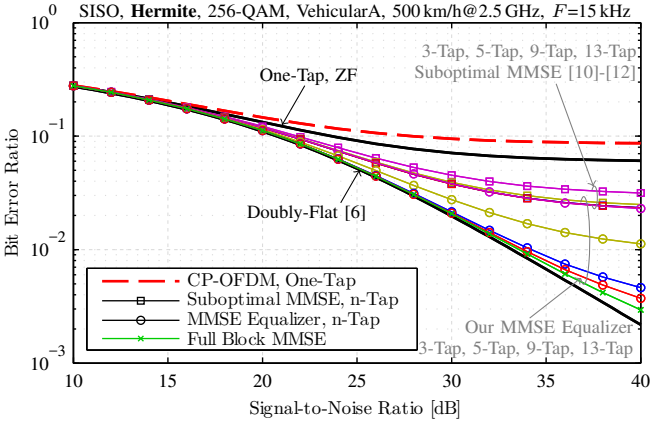

Fig. 5. Compared to the PHYDYAS prototype filter, see Fig. 4, the Hermite pulse shows a higher robustness in time-variant channels.

PHYDYAS prototype filter. As a reference, we also consider CP-OFDM. The upper black curve represent the performance for a one-tap equalizer in our setup while the lower black curve corresponds to a doubly-flat channel [6]. MMSE equalization will result in a performance between these two reference curves. Note that CP-OFDM slightly outperforms FBMC. The equalization method in [10], which uses only neighboring time symbols but ignores neighboring subcarriers, is suboptimal in our scenario. Increasing the number of taps from $|\mathcal{S}| = 5$-taps to $|\mathcal{S}| = 21$-taps only marginally improves the performance. On the other hand, with our equalization method, the performance increases significantly due to the employment of neighboring subcarriers. The 21-tap equalizer even comes close to the full block MMSE equalizer, see (8). For the 3-tap and 5-tap equalizer, it is sufficient to consider only neighboring time symbols. Fig. 3 illustrates which symbols are utilized for the $|\mathcal{S}|$-tap equalizer. To determine the optimal subblock $\mathcal{S}$, we follow loosely the interference distribution of the one-tap equalizer, see Fig. 1. However, this delivers not always the optimal solution as, for example, in case of the 21-tap equalizer.

Fig. 5 shows the BER for the Hermite prototype filter. For a one-tap equalizer, FBMC performs better than CP-OFDM. Overall, the Hermite prototype filter is better suited for high velocity scenarios. In contrast to the PHYDYAS filter, even the 3-tap equalizer of [10] is suboptimal. The optimal 3-tap equalizer utilizes neighboring subcarriers instead of neighboring time-symbols. The 13-tap equalizer already achieves a performance close to that of the full block MMSE equalizer.

The channel model and the prototype filter have a huge impact on which neighboring symbols should be used for the equalization process. For example, in a highly-frequency-selective, but time-invariant, channel, it is usually not necessary to consider neighboring subcarriers for the PHYDYAS prototype filter. For the Hermite prototype filter, on the other hand, we have to utilize neighboring time-symbols and neighboring subcarriers. Thus, for an optimal performance, we always have to check which symbols to include in the equalization process.

Because the Hermite prototype filter performs better than the PHYDYAS prototype filter in high velocity scenarios, we consider only the Hermite prototype filter for the remaining part of the paper.

B. Interference Cancellation

The MMSE equalizer has the big disadvantage of high computational complexity, even if we consider only a small subblock. This is in particular problematic in a time-variant channel, where we have to calculate the equalizer coefficient at every time instant. We therefore propose a simple, yet effective, interference cancellation scheme. Similar as suggested in [17] for OFDM, we can cancel the interference by:

$$\mathbf{y}^{(i+1)} = \mathbf{y} - (\mathbf{D} - \mathrm{diag}\{\mathbf{D}\})\,\hat{\mathbf{x}}^{(i)}. \tag{14}$$

The superscript $(\cdot)^{(i)}$ denotes the i-th iteration and the $\mathrm{diag}\{\mathbf{D}\}$ operator generates a diagonal matrix with the same

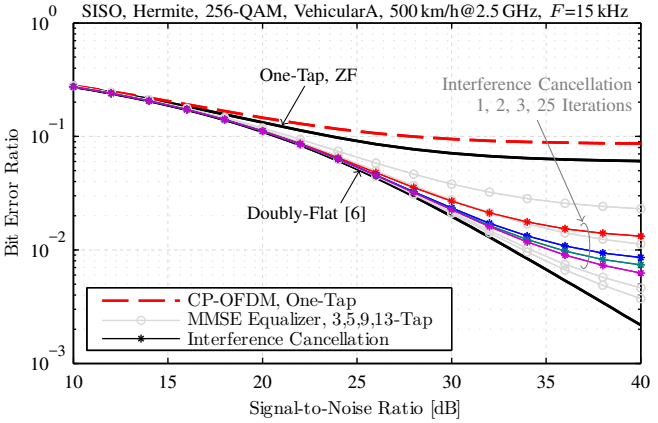

Fig. 6. The main drawback of MMSE equalizers is the high computational complexity. To circumvent this limitation, we propose a simple interference cancellation scheme. For realistic SNR values smaller than 30 dB, we achieve a BER close to the optimum.

diagonal elements as $\mathbf{D}$. Thus $(\mathbf{D} - \mathrm{diag}\{\mathbf{D}\})$ represents all the off-diagonal elements of $\mathbf{D}$. The data estimates are obtained by one-tap equalization according to:

$$\hat{\mathbf{x}}^{(i)} = \mathcal{Q}\left\{\mathrm{diag}\{\mathbf{D}\}^{-1}\,\mathbf{y}^{(i)}\right\}, \tag{15}$$

with $\mathcal{Q}\{\cdot\}$ denoting the quantization operator, that is, nearest neighbor symbol detection. Note that quantization implicitly removes the imaginary interference of FBMC. Our algorithm starts with $\hat{\mathbf{x}}^{(0)}$, representing the conventional (quantized) one-tap equalizer.

Fig. 6 shows the BER over SNR for the interference cancellation scheme in (14) and (15). As a reference (grayed out), we also include the n-tap MMSE equalizers shown in Fig. 5. The BER of interference cancellation lies between the 5-tap equalizer and the 9-tap equalizer. After 2 to 3 iterations, we no longer see a significant performance improvement. Thus, more than 2 to 3 iterations are not necessary, in particular if we want to keep the computational complexity low. Although the cancellation scheme performs not as good as the MMSE equalizer in terms of BER, the performance is still very good, especially for practical relevant SNR values smaller than 30 dB.

Let us now discuss the computational complexity per symbol in more detail. As shown in Fig. 2, only 8 neighboring symbols cause significant interference. Thus, for the first iteration, we only need 9 multiplications (8 + one tap equalizer). For the following iterations, we only require a multiplication if the estimated data symbol $\hat{x}_{l,k}$ has changed. On the other hand, the computational complexity of a 5-tap MMSE equalizer is significantly higher. It requires a matrix inversion of size 10×10 together with additional multiplications, see (11).

IV. Extension to MIMO

So far, we considered only Single-Input and Single-Output (SISO) transmissions, but the extension to MIMO is straightforward thanks to our matrix notation. We only need bigger matrices. Of course, this further increases the computational complexity, making its practical implementation challenging.

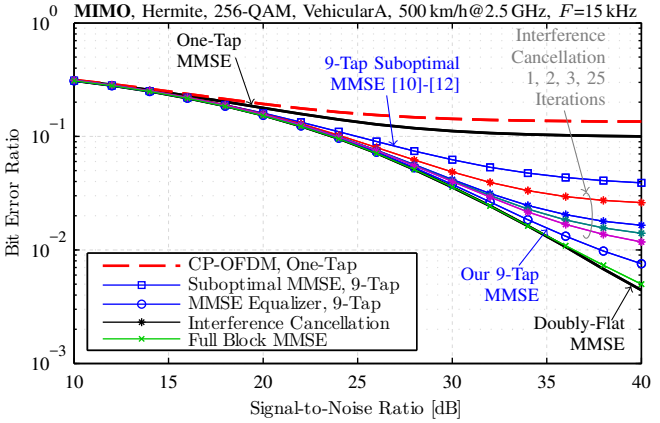

Fig. 7. Our matrix notation allows to straightforwardly extend our equalization method to MIMO. Overall, we observe a similar behavior as in case of SISO. Again, employing neighboring subcarriers improves the performance.

As a theoretical reference, however, the MMSE equalizer is quite useful. Let us consider a 2×2 MIMO transmission system, which can be modeled similar as in (6):

$$\underbrace{\begin{bmatrix}\mathbf{y}_1\\ \mathbf{y}_2\end{bmatrix}}_{\mathbf{y}_\mathrm{M}} = \underbrace{\begin{bmatrix}\mathbf{G}^\mathsf{H}\mathbf{H}_{1,1}\mathbf{G} & \mathbf{G}^\mathsf{H}\mathbf{H}_{1,2}\mathbf{G}\\ \mathbf{G}^\mathsf{H}\mathbf{H}_{2,1}\mathbf{G} & \mathbf{G}^\mathsf{H}\mathbf{H}_{2,2}\mathbf{G}\end{bmatrix}}_{\mathbf{D}_\mathrm{M}} \underbrace{\begin{bmatrix}\mathbf{x}_1\\ \mathbf{x}_2\end{bmatrix}}_{\mathbf{x}_\mathrm{M}} + \begin{bmatrix}\mathbf{G}^\mathsf{H}\mathbf{n}_1\\ \mathbf{G}^\mathsf{H}\mathbf{n}_2\end{bmatrix}. \quad (16)$$

The subscript 1 and 2 now denotes antenna 1 and antenna 2. Similar as in (8), we find the full block MMSE equalizer by:

$$\hat{\mathbf{x}}_\mathrm{M} = \begin{bmatrix}\Re\{\mathbf{D}_\mathrm{M}\}\\ \Im\{\mathbf{D}_\mathrm{M}\}\end{bmatrix}^\mathsf{T} \left(\begin{bmatrix}\Re\{\mathbf{D}_\mathrm{M}\}\\ \Im\{\mathbf{D}_\mathrm{M}\}\end{bmatrix} \begin{bmatrix}\Re\{\mathbf{D}_\mathrm{M}\}\\ \Im\{\mathbf{D}_\mathrm{M}\}\end{bmatrix}^\mathsf{T} + \mathbf{\Gamma}_\mathrm{M} \right)^{-1} \begin{bmatrix}\Re\{\mathbf{y}_\mathrm{M}\}\\ \Im\{\mathbf{y}_\mathrm{M}\}\end{bmatrix} \quad (17)$$

with noise matrix $\mathbf{\Gamma}_\mathrm{M} \in \mathbb{C}^{4LK \times 4LK}$ given by

$$\mathbf{\Gamma}_\mathrm{M} = \frac{P_n}{2} \begin{bmatrix}\Re\{\mathbf{\Lambda}\} & -\Im\{\mathbf{\Lambda}\}\\ \Im\{\mathbf{\Lambda}\} & \Re\{\mathbf{\Lambda}\}\end{bmatrix} \quad \text{with} \quad \mathbf{\Lambda} = \begin{bmatrix}\mathbf{G}^\mathsf{H}\mathbf{G} & \mathbf{0}\\ \mathbf{0} & \mathbf{G}^\mathsf{H}\mathbf{G}\end{bmatrix} \quad (18)$$

In a similar way, we can also find the subblock MIMO MMSE equalizer, as in (11), but applied on the system model in (16). To be consistent with SISO, we count, for an n-tap MIMO equalizer, only the number of taps per antenna. For example, a one-tap MMSE equalizer requires in total four multiplications for the equalization (ignoring the calculation of the equalizer matrix).

The interference cancellation scheme in (14) can also be easily extended to MIMO. The one-tap ZF equalizer in (15) then becomes a one-tap MMSE equalizer, see above.

Fig. 7 shows the BER over the SNR for a 2×2 MIMO system. We observe a similar behavior as in SISO. Considering only neighboring time-symbols, but ignoring neighboring subcarriers, is highly suboptimal. Thus, our 9-tap equalizer performs much better than the 9-tap equalizer proposed in [10]. The interference cancellation scheme also performs relatively good while at the same time the computational complexity is much lower compared to the MMSE equalization.

V. Conclusion

Considering only neighboring time-symbols for the n-tap MMSE equalizer, as usually done in literature for FBMC, is not optimal, especially for the Hermite prototype filter and in a highly time-variant channel. Instead, we utilize neighboring subcarriers as well. The MMSE equalizer has a high computational complexity, so that it is questionable whether it can be employed in practical systems. As a theoretical reference, however, it is quite useful. A simple interference cancellation scheme can solve the complexity issue and achieves a good performance for practical relevant SNR ranges.

Acknowledgment

The financial support by the Austrian Federal Ministry of Science, Research and Economy, the National Foundation for Research, Technology and Development, and the TU Wien is gratefully acknowledged. The research has been co-financed by the Czech Science Foundation, Project No. 17-18675S "Future transceiver techniques for the society in motion," and by the Czech Ministry of Education in the frame of the National Sustainability Program under grant LO1401.

References

[1] R. Nissel, S. Schwarz, and M. Rupp, "Filter bank multicarrier modulation schemes for future mobile communications," *IEEE Journal on Selected Areas in Communications*, 2017, to appear.

[2] R. Nissel, S. Caban, and M. Rupp, "Experimental evaluation of FBMC-OQAM channel estimation based on multiple auxiliary symbols," in *IEEE Sensor Array and Multichannel Signal Processing Workshop (SAM)*, Rio de Janeiro, Brazil, July 2016.

[3] R. Nissel and M. Rupp, "Enabling low-complexity MIMO in FBMC-OQAM," in *IEEE Globecom Workshops (GC Wkshps)*, Dec 2016.

[4] R. Nissel, E. Zöchmann, M. Lerch, S. Caban, and M. Rupp, "Low-latency MISO FBMC-OQAM: It works for millimeter waves!" in *IEEE International Microwave Symposium*, Honolulu, Hawaii, June 2017.

[5] R. Nissel, J. Blumenstein, and M. Rupp, "Block frequency spreading: A method for low-complexity MIMO in FBMC-OQAM," in *IEEE International Workshop on Signal Processing Advances in Wireless Communications (SPAWC)*, Sapporo, Japan, Jul. 2017.

[6] R. Nissel and M. Rupp, "OFDM and FBMC-OQAM in doubly-selective channels: Calculating the bit error probability," *IEEE Communications Letters*, 2017, accepted for publication.

[7] X. Mestre and D. Gregoratti, "Parallelized structures for MIMO FBMC under strong channel frequency selectivity." *IEEE Trans. Signal Processing*, vol. 64, no. 5, pp. 1200–1215, 2016.

[8] M. Caus and A. I. Pérez-Neira, "Transmitter-receiver designs for highly frequency selective channels in MIMO FBMC systems," *IEEE Transactions on Signal Processing*, vol. 60, no. 12, pp. 6519–6532, 2012.

[9] M. Bellanger, "FS-FBMC: An alternative scheme for filter bank based multicarrier transmission," in *IEEE International Symposium on Communications Control and Signal Processing (ISCCSP)*, 2012.

[10] D. S. Waldhauser, L. G. Baltar, and J. A. Nossek, "MMSE subcarrier equalization for filter bank based multicarrier systems," in *IEEE SPAWC*, 2008.

[11] A. Ikhlef and J. Louveaux, "Per subchannel equalization for MIMO FBMC/OQAM systems," in *IEEE Pacific Rim Conference on Communications, Computers and Signal Processing*, 2009.

[12] L. Marijanović, S. Schwarz, and M. Rupp, "MMSE equalization for FBMC transmission over doubly-selective channels," in *IEEE International Symposium on Wireless Communication Systems*, 2016.

[13] R. Nissel, E. Zöchmann, and M. Rupp, "On the influence of doubly-selectivity in pilot-aided channel estimation for FBMC-OQAM," in *IEEE Vehicular Technology Conference (VTC Spring)*, 2017, pp. 1–5.

[14] M. Bellanger, D. Le Ruyet, D. Roviras, M. Terré, J. Nossek, L. Baltar, Q. Bai, D. Waldhauser, M. Renfors, T. Ihalainen *et al.*, "FBMC physical layer: a primer," *PHYDYAS, January*, 2010.

[15] R. Haas and J.-C. Belfiore, "A time-frequency well-localized pulse for multiple carrier transmission," *Wireless Personal Communications*, vol. 5, no. 1, pp. 1–18, 1997.

[16] R. Nissel and M. Rupp, "On pilot-symbol aided channel estimation in FBMC-OQAM," in *IEEE International Conference on Acoustics, Speech and Signal Processing (ICASSP)*, Shanghai, China, March 2016.

[17] A. F. Molisch, M. Toeltsch, and S. Vermani, "Iterative methods for cancellation of intercarrier interference in OFDM systems," *IEEE Transactions on Vehicular Technology*, vol. 56, no. 4, pp. 2158–2167, 2007.